INORGANIC CHEMISTRY
FRONTIERS

RESEARCH ARTICLE

View Article Online
View Journal | View Issue

Cite this: *Inorg. Chem. Front.*, 2022, **9**, 2221

A quantitative single-nanowire study on the plasmonic enhancement for the upconversion photoluminescence of rare-earth-doped nanoparticles†

Xin Su, Li-Wei Chen, Zhejiaji Zhu, Jiani Li, Nan Zhang, Tong-An Bu, Yu-Chen Hao, Wen-Yan Gao, Di Liu, Si-Qian Wu, Zi-Long Yu, Hui-Zi Huang and An-Xiang Yin *

Local surface plasmon resonance (LSPR) modulation represents a promising way for enhancing upconversion photoluminescence (UCPL). The study on the coupling mechanism of LSPR and UCPL is of great importance for both fundamental research and practical applications. However, general protocols based on the collective signals of mixed samples always suffered from the wide distributions of samples and inevitable interferences from the scattering and/or absorption of the surrounding samples, preventing the mechanism study with high accuracy and fidelity. Herein, we report a high-accuracy and quasi *in situ* study on the coupling of LSPR and UCPL in a single nanowire way. We chemically attached rare-earth (RE)-doped upconversion nanoparticles to Ag nanowires (UCNPs/AgNWs) and finely tuned their spectrum match, spacers, and surface coverages. We also developed a quasi *in situ* selective etching method to achieve LSPR–UCPL coupling on a single-nanowire scale with high accuracy. Our results proved that the LSPR enhancement of UCPL showed a strong dependence on the spectrum match and the distances between the LSPR and UCPL units. Compared with collecting average signals from the mixed samples, our single-nanowire method provides a superior approach to quantifying the LSPR–UCPL coupling with high accuracy and fidelity. These strategies may find more applications in the study of LSPR and/or UCPL materials, leading to a deeper understanding of the coupling mechanism of surface plasmon and photoluminescence processes.

Received 11th January 2022,
Accepted 22nd March 2022

DOI: 10.1039/d2qi00084a

rsc.li/frontiers-inorganic

1. Introduction

Lanthanide-doped upconversion nanoparticles (UCNPs) can convert near-infrared light to visible light *via* a multi-photon absorption process.[1–3] Owing to the rich energy level structures for the 4f electrons of rare-earth (RE) elements, such RE-doped UCNPs exhibit unique optical properties (*e.g.*, large anti-Stokes shifts, narrow emission peaks, long emission lifetimes, and low background interference)[4–8] and have broad applications in biosensing,[9,10] bioimaging,[11,12] and photothermal therapy.[13,14] However, due to the small intrinsic absorption cross-sections and the low quantum efficiencies for 4f–4f transitions, UCNPs usually suffer from low overall upconversion photoluminescence (UCPL) efficiency. Therefore, enhancing the UCPL efficiency has turned out to be a critical task for researchers for decades.

Extensive methods have been developed to enhance the UCPL efficiency, including optimizing host materials and/or dopant concentrations,[15–18] constructing core–shell nanostructures,[19–21] using organic sensitizers,[22,23] employing plasmon enhancement,[24–26] *etc*. For example, RE fluoride NPs (*e.g.*, $NaYF_4$ and $NaGdF_4$) have proven to be efficient hosts for UCPL due to their low phonon energies,[27,28] while forming core–shell structures with doped cores, and inert shells, which can passivate surface defects to further enhance the UCPL efficiency.[22,29] Meanwhile, localized surface plasmon resonance (LSPR) effects can significantly enhance the local electromagnetic (EM) field surrounding the metal, which can thereby couple with the EM field of emitters located in evanescently confined LSPR fields.[30–33] Upon rational modulation, the UCPL efficiency can be enhanced effectively through two plausible mechanisms, including the local electric field amplification, and/or the enhanced radiative decay rate.[28,34]

Ministry of Education Key Laboratory of Cluster Science, Beijing Key Laboratory of Photoelectronic/Electrophotonic Conversion Materials, Advanced Technology Research Institute (Jinan), School of Chemistry and Chemical Engineering, Beijing Institute of Technology, Beijing 100081, China. E-mail: yin@bit.edu.cn

† Electronic supplementary information (ESI) available. See DOI: https://doi.org/10.1039/d2qi00084a

The critical parameters for the LSPR enhancement of UCPL include the spectrum match and the distances between the LSPR surfaces and the UCPL cores, which have been widely studied and proved by physically coupling UCNPs with zero, one, and two-dimensional (0D, 1D, and 2D) LSPR materials with controlled spatial distances.[12,34–38] For instance, as a kind of typical LSPR material, 1D Ag nanowires (AgNWs) could be assembled with UCNPs through solvent-evaporation induced self-assembly or spin coating to study their enhancement effect on UCPL.[39–42] However, previous protocols usually could only provide collective signals from the large assemblies of many UCNPs and AgNWs, which may vary from each other in morphologies, sizes, and emission/scattering spectra. In sharp contrast, the precise control and the quantitative study of the influences of spectrum match and spatial distance on the LSPR enhancement of UCPL could be readily achieved if we can study the combination and the photoluminescence properties of UCNPs and AgNWs in a single-nanowire manner.

Here, we present a 3-mercaptopropionic acid (MPA)-assisted chemical assembly of UCNPs with controllable emission spectra and shell thickness and AgNWs with adjustable diameters to obtain UCNPs/AgNW hybrids with precisely tunable LSPR–UCPL spectrum match, distances, and surface UCNP coverages (Fig. 1a–d). A head-to-head quasi *in situ* optical characterization method on a single-nanowire scale was also developed by quasi *in situ* selective etching of the AgNWs of UCNPs/AgNWs with the help of the markers on silica wafers (Fig. 1e). Compared with the collective optical signals from conventional samples (solid phase and solution), such single-NW-based optical characterization studies could finely explore the effects of LSPR–UCPL spectrum match, distances, and UCNP coverages on LSPR–UCPL coupling (Fig. 1f–h). Such a head-to-head comparison between the single UCNPs/AgNW (before etching) and the remaining UCNPs (after etching) revealed that plasmonic AgNWs could significantly enhance the UCPL intensity of Tm-/Er-doped UCNPs. Our results also proved that the enhancement factors (EFs) are highly dependent on the spectrum match and the spatial distances between the LSPR surfaces and the UCPL cores.

2. Experimental

2.1 Preparation and surface modification of UCNPs

UCNPs were prepared through a thermal decomposition approach with modifications.[43] Typical RE-doped UCPL nanoparticles, β-$NaGdF_4$:50%Yb,1%Tm (denoted as β-Tm), β-$NaGdF_4$:50%Yb,0.5%Tm, β-$NaGdF_4$:50%Yb,1.5%Tm and β-$NaGdF_4$:20%Yb,2%Er (denoted as β-Er), were prepared by reacting sodium with RE trifluoroacetic acetates in a mixture of oleic acid (OA), oleylamine (OM), and 1-octadecene (ODE). These UCPL cores were then coated with undoped β-$NaYF_4$

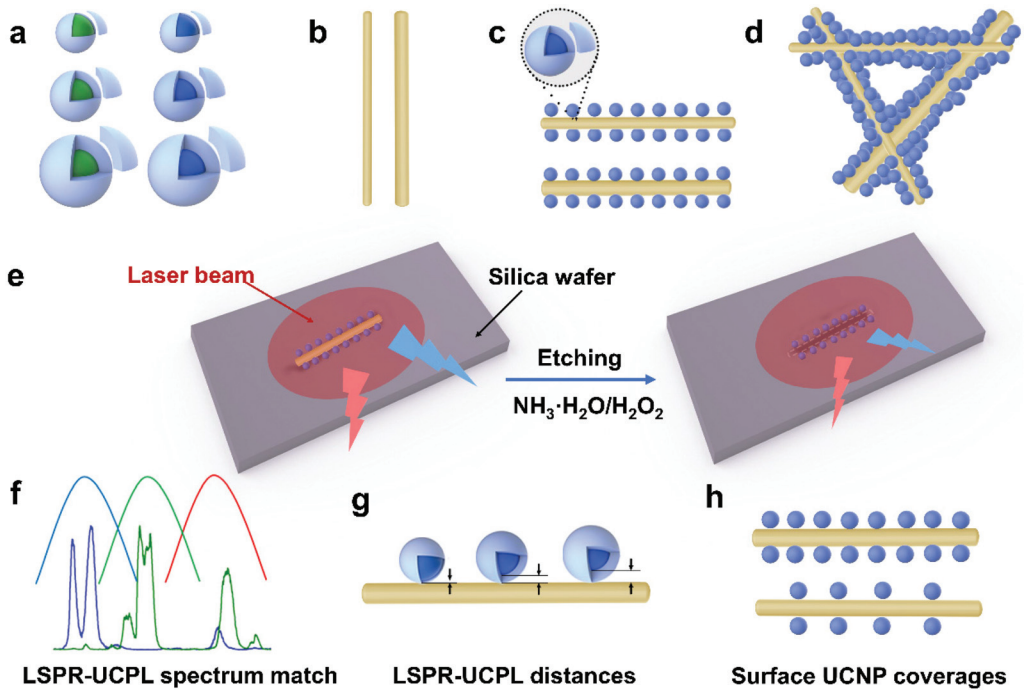

Fig. 1 Schematic illustration for the design and optical characterization of UCNPs/AgNWs with tunable LSPR–UCPL spectrum match, distances, and surface UCNP coverages. (a) UCNPs consisting of doped cores with tunable emission spectra and undoped shells with controllable thicknesses. (b) AgNWs with tunable diameters. (c) UCNPs/AgNW hybrids with tunable LSPR–UCPL spectrum match, distances, and surface UCNP coverages. (d) Randomly aggregated samples. (e) Single nanowire-based quasi *in situ* optical measurements. The AgNW can be selectively removed with no significant influence on UCNPs. (f–h) The parameters that could be modulated for the study of LSPR–UCPL coupling. (f) The spectrum match of the AgNW and UCNPs. (g) The distances between the AgNW surface and the UCPL cores. (h) The surface coverages of UCNPs on the AgNW.

shells with thicknesses controlled by adjusting the amounts of precursors for the β-$NaYF_4$ shells. The as-obtained core–shell UCNPs were separated, washed, and redispersed in cyclohexane for further use and characterization studies.

A two-step-ligand-exchange method was used to modify the surface-adsorbed surfactants of the UCNPs to obtain MPA-functionalized UCNPs (MPA–UCNPs), which can be readily dispersed in dimethylformamide (DMF) and exhibit high affinity for AgNWs owing to their thiolate functional groups.[44] The core–shell UCNPs were first treated with $NOBF_4$, redispersed in DMF, and then incubated with appropriate amounts of MPA to obtain hydrophilic MPA–UCNPs.

2.2 Assembly of MPA–UCNPs with polyvinyl pyrrolidone (PVP)-modified AgNWs (PVP-AgNWs)

AgNWs were synthesized by the reported PVP-assisted polyol process with modifications.[45] The as-prepared PVP-AgNWs were dispersed in DMF, mixed with the DMF dispersion of MPA–UCNPs, and shaken at room temperature to obtain hybrid UCNPs/AgNWs.

Notably, the spectrum match between the UCNPs and the AgNWs could be controlled by the dopants (*i.e.*, Tm^{3+} and Er^{3+}) of UCNPs and the diameters of AgNWs. UCNPs/AgNWs with different activator (Tm^{3+}) doping concentrations could be obtained by controlling the Tm^{3+} doping ratio in Tm-doped UCNPs. The distances between the UCPL cores and the LSPR surfaces (of AgNWs) could be modulated by the shell thickness of UCNPs. The surface coverages of the UCNPs on AgNWs could be easily adjusted by the ratio of the DMF dispersions of AgNWs and UCNPs. The as-obtained UCNPs/AgNW hybrids were centrifuged, washed, and redispersed in DMF for further use.

2.3 Optical set-up

The optical images of the UCNPs, AgNWs, and their hybrid structures were collected using an upright optical microscope (DM2700 M, Leica) with a long work distance 5× objective with a numerical aperture (NA) of 0.15 and a 50× objective with a NA of 0.55 in bright field (BF) and dark field (DF) modes (Fig. S1†). A quartz-tungsten-halogen lamp (100 W, Leica) was used to collect the DF images of AgNWs, and a diode 980 nm laser (5 W, Hi-Tech Optoelectronics Co., Ltd China) was used to stimulate the UCNPs. A spectrometer (iHR550, Horiba) and an electron-multiplying charge-coupled device (EMCCD, Synapse EM, Horiba) were coupled with a microscope by optical fibers to collect the scattering and emission spectra of the specimen.

2.4 Optical measurements of single nanowires

A diluted dispersion of UCNPs/AgNWs was drop-cast onto silica/silicon wafers with pre-deposited gold markers to obtain sparsely deposited UCNPs/AgNW samples for the acquisition of their optical signals on a single-nanowire scale. The accurate positioning of the specific sample was achieved by the alignment of the optical images and the scanning electron microscopy (SEM) images of the samples with the help of the markers on the silica wafers. The selective illumination and spectrum acquisition of a single nanowire were achieved by adjusting the spot sizes of the incident light, the diameters of the optical fiber, and the slit of the spectrometer, avoiding the interferences from nearby samples. Notably, after the optical measurements, the AgNW part in the hybrid nanowire could be selectively etched by ammonia and hydrogen peroxide, while the UCNPs could be preserved on the silica wafer with unchanged morphologies and locations (see the ESI† for more details). As a result, we can acquire the UCPL signals of these UCNPs and make a head-to-head comparison between the single UCNPs/AgNW hybrid (before etching) and the preserved UCNPs (after etching) to reveal the LSPR enhancement on UCPL in a quasi *in situ* manner.

3. Results and discussion

3.1 Attaching UCNPs to AgNWs

As revealed by the transmission electron microscopy (TEM) and SEM images, a series of monodispersed UCNPs with (0.5%, 1%, and 1.5%) Tm/2%Er-doped cores and undoped shells with tunable thicknesses were obtained by solution synthesis (Fig. 2a and b and Fig. S2, S3, and S4†). AgNWs with diameters of 80–130 nm and lengths of 8–12 μm were obtained by the polyol process (Fig. 2c and Fig. S5†). As shown in Fig. 2d–f, after the surface modification, the MPA-capped UCNPs consisting of 1%Tm-doped cores and undoped shells with a thickness of 2.1 ± 0.2 nm (denoted as Tm@2.1 hereafter, where the number 2.1 represents undoped shells with average thickness of 2.1 nm) could be uniformly attached to AgNWs. TEM and high-angle annular dark-field scanning TEM (HAADF-STEM) images demonstrated that UCNPs were tightly attached on the surfaces of AgNWs (Fig. 2e and f), suggesting that the distances between the UCPL cores and the LSPR surfaces could

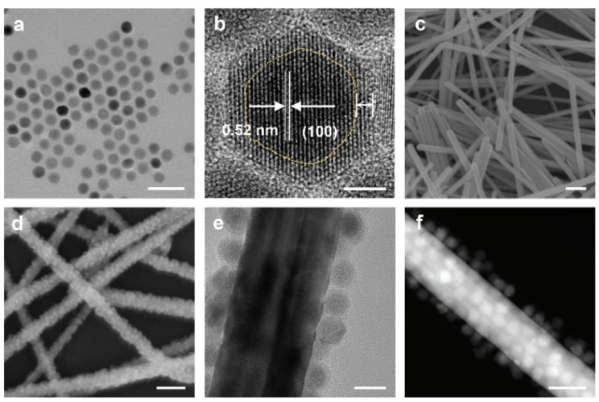

Fig. 2 Structure and morphology characterization of Tm@2.1 NPs, AgNWs, and the Tm@2.1/AgNW hybrids. (a and b) TEM and high-resolution TEM images of Tm@2.1 NPs. The boundary of the doped $NaGdF_4$ core and the undoped $NaYF_4$ shell is highlighted for eye guidance in (b). (c) SEM image of AgNWs. (d) SEM, (e) TEM, and (f) HAADF-STEM images of Tm@2.1/AgNW hybrids. Scale bars: (a) 100 nm, (b) 5 nm, (c) 400 nm, (d) 200 nm, (e) 20 nm, and (f) 50 nm.

be easily tuned by the thickness of the undoped $NaYF_4$ shells (Fig. S6 and S7†) and the UCNP coverage could be modulated by the ratios between the UCNPs and the AgNWs during the assembly process (Fig. S8†). In addition, Tm-doped UCNPs with different Tm^{3+} doping concentrations were also attached to the surface of AgNWs (Fig. S9†). In contrast, UCNPs without MPA modification were hardly attached to the surface of Ag NWs (Fig. S10†), suggesting that MPA could play a vital role in the assembly of UCNPs/AgNW hybrid structures due to the high affinity between the thiol groups and the surface Ag atoms.[46]

3.2 Spectrum match

We then attached the Tm@2.1 NPs to AgNWs with different diameters to reveal the interaction between the Tm@2.1 NPs and the AgNWs with different scattering spectra in a single nanowire manner (Fig. 3). For instance, a hybrid nanowire of Tm@2.1 NPs and one AgNW with a diameter of 55 nm (determined by SEM) could be clearly observed and positioned in the DF optical image (Fig. 3a) due to their strong scattering centered at about 550 nm (Fig. 3e, grey line). Notably, assisted by the markers on the silica wafer, we can also observe the same hybrid nanowire in the SEM image, showing that the Tm@2.1 NPs were evenly attached to the AgNW (Fig. 3b). Under the stimulation of a 980 nm laser, the Tm@2.1/AgNW exhibited three major upconversion emission bands located at about 445, 470, and 643 nm (Fig. 3e, red line), which correspond to the $^1D_2$ to $^3F_4$, $^1G_4$ to $^3H_6$, and $^1G_4$ to $^3F_4$ transitions of Tm^{3+}, respectively.[2] After acquiring the UCPL and scattering spectra of the Tm@2.1/AgNW, the specimens were immersed in the enchant consisting of ammonia and hydrogen peroxide to selectively remove the AgNW with the Tm@2.1 NPs preserved on the silica wafer (Fig. 3c and d). Notably, control experiments proved that the etching treatment showed negligible influence on the UCPL of pure Tm@2.1 NPs (Fig. S11†).

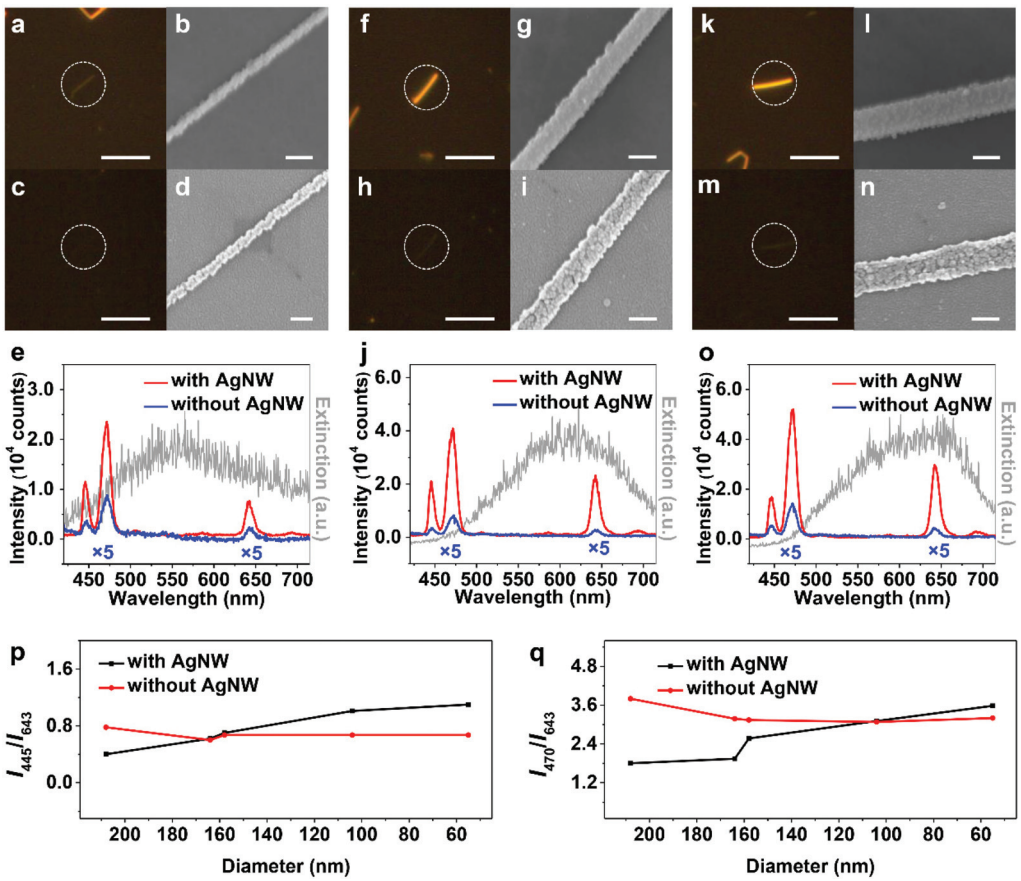

Fig. 3 LSPR-enhanced UCPL performance of Tm@2.1/AgNWs with different diameters. (a–d) Optical DF and SEM images of one hybrid nanowire of Tm@2.1/AgNW (diameter: 55 nm) before (a and b) and after (c and d) etching. Note that the AgNW was selectively removed and the UCNPs remained after the etching treatment. (e) The UCPL spectra of the Tm@2.1/AgNW shown in a–d before (red) and after (blue) selective etching (left axis), and the extinction spectrum (grey) of the Tm@2.1/AgNW before etching (right axis). (f–i) Optical DF and SEM images of one hybrid nanowire of Tm@2.1/AgNW (diameter: 164 nm) before (f and g) and after (h and i) etching. (j) The UCPL spectra of the Tm@2.1/AgNW shown in f–i before (red) and after (blue) selective etching, and the extinction spectrum (grey) of the Tm@2.1/AgNW before etching. (k–n) Optical DF and SEM images of one hybrid nanowire of Tm@2.1/AgNW (diameter: 208 nm) before (k and l) and after (m and n) etching. (o) The UCPL spectra of the Tm@2.1/AgNW shown in k–n before (red) and after (blue) selective etching, and the extinction spectrum (grey) of the Tm@2.1/AgNW before etching. (p) The I_{445}/I_{643} and (q) I_{470}/I_{643} ratios for Tm@2.1/AgNWs with different diameters before (with the AgNW) and after (without the AgNW) the selective etching of AgNWs. Scale bars: (a, c, f, h, k and m) 10 μm and (b, d, g, i, l and n) 200 nm.

Therefore, with the selective etching of the AgNW, we can monitor the UCPL of the remaining Tm@2.1 NPs and make a head-to-head comparison between the UCPL spectra of the hybrid Tm@2.1/AgNW and the remaining Tm@2.1 NPs to reveal the effects of LSPR on UCPL in a quasi *in situ* way. As revealed by the DF image (Fig. 3c), no typical LSPR scattering signals could be observed from the same spot on the silica wafer. Compared with the pristine sample of Tm@2.1/AgNW before selective etching, the scattering peak of the etched sample almost completely disappeared (Fig. S12†). In addition, as shown in Fig. S13,† the EDX mapping showed that no apparent signals for Ag could be found for the selectively etched samples. The results all suggested that the AgNW could be removed by the selective etching process. The SEM images (Fig. 3d and Fig. S14†) also confirmed the removal of the AgNW and the preservation of Tm@2.1 UCNPs. Interestingly, the remaining Tm@2.1 UCNPs exhibited a significantly decreased UCPL emission under similar stimulation conditions (Fig. 3e, blue line). The emissions at 445, 470, and 643 nm for the hybrid Tm@2.1/AgNW were about 21, 14, and 13 times that for the remaining Tm@2.1 UCNPs, respectively (Fig. 3e and Table S1†). Therefore, the coupling of LSPR would significantly enhance the three primary UCPL emissions of the Tm-doped core with a spacer thickness of about 2.1 nm. As a result, the intensity ratios between the two blue emission peaks and the red emission (*i.e.*, I_{445}/I_{643} and I_{470}/I_{643}) were increased from 0.67 and 3.20 to 1.10 and 3.58, respectively, showing the different EFs for different Tm^{3+} emission bands due to the different match degrees between the LSPR scattering spectra and the emission bands of the Tm^{3+}-doped UCPL cores (Fig. 3e).

Similar LSPR enhancement effects could also be observed for the hybrid nanowires of Tm@2.1 UCNPs and AgNWs with different diameters and scattering spectra (Fig. 3f–o, Fig. S15 and S16 and Table S1†). For example, the coupling of the single AgNW (diameter:164 nm) and the scattering spectrum centered at 610 nm would enhance the emissions at 445, 470, and 643 nm by 49, 29, and 48 times, respectively (Fig. 3f–j and Fig. S15†). The single AgNW (diameter: 208 nm) and the scattering peak at about 650 nm would promote the Tm^{3+} emissions at 445, 470, and 643 nm by 25, 23, and 48 times, respectively (Fig. 3k–o and Fig. S16†).

Although the three emissions of the Tm-doped cores embedded in 2.1 nm shells could all be significantly enhanced by AgNWs with diameters from 55 to 208 nm, the EFs varied for different emission peaks and thus resulted in the increased or decreased blue/red ratios. For AgNWs with smaller diameters, the blue emissions were enhanced more significantly, while AgNWs with larger diameters exhibited larger EFs for red emissions. As a result, a clear trend in the dependence of the emission blue/red ratio (*i.e.*, I_{445}/I_{643} and I_{470}/I_{643}) on the diameters of AgNWs could be observed on all the studied samples (Fig. 3p and q and Fig. S17 and S18†). That is, with the decrease of the diameters of AgNWs, their LSPR scattering peaks would gradually shift to a shorter wavelength (Fig. 3a–o and Fig. S19†).[47–49] The blue-shifted LSPR resonances would couple more with the $^1D_2$ to $^3F_4$ and $^1G_4$ to $^3H_6$ transitions of Tm^{3+}, resulting in a relatively higher enhancement in the blue emissions.

A similar LSPR-induced UCPL enhancement was also observed for the hybrid nanowires of Tm@2.6/AgNWs with different doping concentrations (where the number 2.6 represents the undoped shells with an average thickness of 2.6 nm). When the Tm^{3+} doping concentration was 0.5%, the emission intensity of 0.5%Tm@2.6 NPs was enhanced by 10 times due to the presence of scattering of the AgNW (diameter: 66 nm) (Fig. S20†). The single AgNW (diameter: 41 nm) would heighten the emissions by 8 times for 1.5%Tm@2.6 NPs (Fig. S21†).

A similar LSPR enhancing effect could also be applied to Er^{3+}-doped UCNPs, which showed two characteristic emission peaks in the green region ($^2H_{11/2}$ to $^4I_{15/2}$ and $^4S_{3/2}$ to $^4I_{15/2}$) and one in the red region ($^4F_{9/2}$ to $^4I_{15/2}$).[2] As shown in Fig. 4, we also attached MPA-modified UCNPs consisting of Er-doped cores and inert shells with a thickness of 2.6 ± 0.3 nm (denoted as Er@2.6) to AgNWs with different diameters to reveal the effects of LSPR on different emission bands of Er-doped UCNPs. Similarly, single nanowire studies revealed that the UCPL of Er-doped cores embedded in 2.6 nm thick shells could be generally enhanced by the LSPR of the single AgNWs with different diameters despite the relatively lower EFs (Fig. 4, Fig. S22–26, and Table S2†). For instance, Er@2.6 NPs could be coupled with one single AgNW (diameter: 53 nm) and an intense scattering spectrum centered at 565 nm was observed (Fig. 4a–e and Fig. S22†). A head-to-head comparison between the UCPL of the Er@2.6/AgNW hybrid and the remaining Er@2.6 NPs after the selective etching of AgNWs revealed that the UCPL emissions at 520, 540, and 655 nm were magnified by the AgNWs with factors of 5.3, 4.5, and 4.8, respectively (Fig. 4e and Table S2†).

The enhancement of the UCPL of Er-doped NPs was also dependent on the diameter of AgNWs. The MPA-modified Er@2.6 NPs were coupled with single AgNWs with different diameters and the scattering spectra were obtained to reveal their UCPL properties with/without the enhancement by the AgNWs (Fig. 4f–o, Fig. S23 and S24, and Table S2†). The AgNW with a diameter of 60 nm could enhance the emissions at 520, 540, and 655 nm by 5.5, 5.7, and 7.0 times, respectively (Fig. 4f–j and Fig. S23†). The other AgNW with a larger diameter of 200 nm could strengthen the emissions at 520, 540, and 655 nm by 2.1, 1.8, and 4.5 times, respectively (Fig. 4k–o and Fig. S24†).

As shown in Fig. 4e, j and o, the enhancement of the green and red emissions was highly dependent on the scattering spectra of AgNWs, which were regulated by their diameters (Fig. S19†).[47–49] AgNWs with larger diameters would exhibit a scattering spectrum centered in the red region and therefore enhance the red emissions more, while AgNWs with smaller diameters would show a blue-shifted scattering spectrum and promote the green emissions with higher EFs. A clear trend in the diameter dependence of the EFs for emissions at different wavelengths could be observed when plotting the intensity

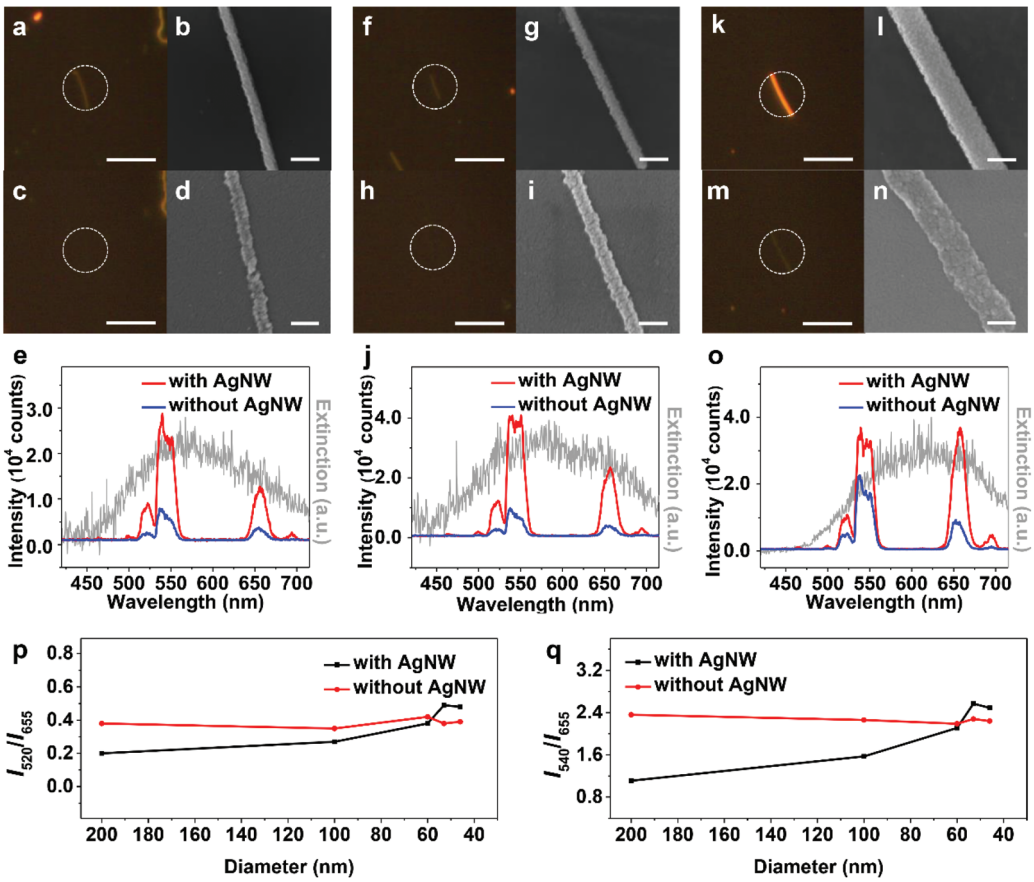

Fig. 4 LSPR-enhanced UCPL performance of Er@2.6/AgNWs with different diameters. (a–d) Optical DF and SEM images of one hybrid nanowire of Er@2.6/AgNW (diameter: 53 nm) before (a and b) and after (c and d) etching. (e) The UCPL spectra of the Er@2.6/AgNW shown in a–d before (red) and after (blue) selective etching (left axis), and the extinction spectrum (grey) of the Er@2.6/AgNW before etching (right axis). (f–i) Optical DF and SEM images of one hybrid nanowire of Er@2.6/AgNW (diameter: 60 nm) before (f and g) and after (h and i) etching. (j) The UCPL spectra of the Er@2.6/AgNW shown in f–i before (red) and after (blue) selective etching, and the extinction spectrum (grey) of the Er@2.6/AgNW before etching. (k–n) Optical DF and SEM images of one hybrid nanowire of Er@2.6/AgNW (diameter: 200 nm) before (k and l) and after (m and n) etching. (o) The UCPL spectra of the Er@2.6/AgNW shown in f–i before (red) and after (blue) selective etching, and the extinction spectrum (grey) of the Er@2.6/AgNW before etching. (p) The I_{520}/I_{655} and (q) I_{540}/I_{655} ratios for Er@2.6/AgNWs with different diameters before (with the AgNW) and after (without the AgNW) the selective etching of AgNWs. Scale bars: (a, c, f, h, k and m) 10 μm and (b, d, g, i, l and n) 200 nm.

ratios for the green/red emissions (*i.e.*, I_{520}/I_{655} and I_{540}/I_{655}) of Er@2.6/AgNW hybrids against the diameter of single AgNWs (Fig. 4p and q and Fig. S25 and S26†). Both the I_{520}/I_{655} and I_{540}/I_{655} were increased with the decreasing diameter of AgNWs, also suggesting the vital role of spectrum match in the LSPR enhancement of UCPL.

According to previous theoretical and experimental studies, the promotion of UCPL by LSPR will follow two possible processes: (1) increasing the excitation rate by the local electric field amplification when the excitation band of UCNPs overlaps with the LSPR, and/or (2) increasing the emission rate by surface-plasmon-coupled emission when the emission bands overlap with the LSPR. Based on the quasi *in situ* head-to-head comparison of the UCPL from the Tm- and Er-doped core/shell UCNPs and their hybrid structures with single AgNWs, we found that the EFs were strongly dependent on the spectrum match between the UCPL emissions and the scattering spectra of AgNWs, which are regulated by their diameters. Our work, in a single-nanowire manner with high accuracy and fidelity, clearly suggested that the coupling of LSPR and UCPL emission bands with an appropriate spectrum match would result in enhanced emission intensity due to the faster radiative decay rate.[31]

3.3 Shell thickness

The distances between the LSPR surfaces and the UCPL cores could be readily tuned by the thickness of the undoped shells of UCNPs to reveal their vital role in the coupling of LSPR and UCPL. In addition, we also employed the blue-to-red ratio (*i.e.*, $I_{445+470}/I_{643}$) as an internal standard to reveal the coupling effectiveness. As shown in Fig. 5a–c and Fig. S6,† uncoated β-Tm NPs and a series of Tm-doped cores coated with inert $NaYF_4$ shells with thicknesses ranging from 2.1 to 15.4 nm were attached to AgNWs to reveal the influence of LSPR on their UCPL properties. As shown in Fig. S27,† the LSPR enhancement of the UCPL of the bare β-Tm NPs was much

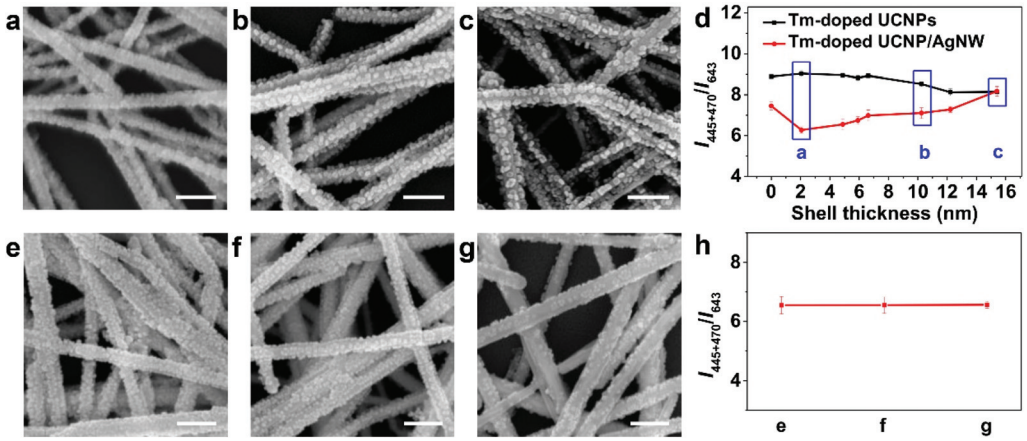

Fig. 5 LSPR–UCPL coupling behavior of Tm-doped UCNPs/AgNWs with varied distances and surface UCNP coverages. (a–c) SEM images of Tm-doped UCNPs/AgNWs with varied undoped $NaYF_4$ shell thicknesses of (a) 2.1 nm, (b) 10.3 nm, and (c) 15.4 nm. (d) The $I_{445+470}/I_{643}$ ratios for upconversion emissions of Tm-doped UCNPs with different $NaYF_4$ shell thicknesses (black) and their corresponding hybrids with AgNWs (*i.e.*, UCNPs/AgNWs) (red). The error bars indicate the standard deviation for five and fifteen independent samples of UCNPs and UCNPs/AgNWs, respectively. (e–g) SEM images of Tm@4.9/AgNWs with different surface coverages of the UCNPs on AgNWs. (h) The statistical $I_{445+470}/I_{643}$ ratios for single Tm@4.9/AgNW hybrids shown in panels e–g. The error bars indicate the standard deviation for fifteen independent samples. Scale bars: 300 nm.

smaller than that of the aforementioned Tm@2.6 NPs. Moreover, the statistical results (Fig. 5d and Fig. S28†) demonstrated that the $I_{445+470}/I_{643}$ ratio was generally decreased by the AgNWs (whose scattering spectra were centered at about 620 nm) when the shell thickness was smaller than 15 nm, indicating that the red emission of Tm^{3+} would be enhanced more than the blue emission due to the greater spectrum overlap between the LSPR of AgNWs and the UCPL of Tm-doped UCNPs in the red region. Notably, a clear trend showed that the LSPR-induced decrease of the blue-to-red ratio ($I_{445+470}/I_{643}$) gradually decreased with the growth of the shell thickness. Especially, when the shell thickness was increased to 15.4 ± 0.7 nm, the $I_{445+470}/I_{643}$ ratio was almost identical for the Tm@15.4 UCNPs and Tm@15.4/AgNW hybrids. A similar trend was also observed in the UCPL of uncoated β-Er NPs and Er-doped cores coated with inert $NaYF_4$ shells (with the shell thicknesses varied from 2.6 to 9.8 nm) with/without the coupling of LSPR from AgNWs (Fig. S7, S29 and S30†). The LSPR-induced increase of the green-to-red ratio ($I_{520+540}/I_{655}$) also gradually decreased with the increasing shell thickness. That is, our results demonstrated that the coupling of LSPR and UCPL was very sensitive to the distances between the LSPR surfaces and the UCPL cores, which could be attributed to the exponentially decayed LSPR field in the vertical direction away from the surfaces of noble metals.[50] Therefore, the LSPR-enhancement of UCPL by the AgNWs was highly dependent on the distances between the AgNW surfaces and the Tm-/Er-doped UCPL cores, and an appropriate shell thickness (typically < 10 nm) would be of vital importance.

3.4 Surface coverage

A series of UCNPs/AgNW hybrids with different surface coverages of UCNPs on AgNWs were prepared by adjusting the concentrations of UCNPs and AgNWs during the assembly process. As shown in Fig. 5e–g and Fig. S8,† Tm-doped cores embedded in 4.9 nm shells and Er-doped cores coated with 2.6 nm shells were evenly attached to the AgNWs with different surface coverages (≤1 monolayer, ML). The surface coverage of UCNPs decreased with the reduced concentrations of UCNPs in the assembly process. However, as shown in Fig. 5h, the statistical results demonstrated that the $I_{445+470}/I_{643}$ ratio did not show any noticeable difference for Tm@4.9/AgNW samples with different surface UCNP coverages. Similarly, the $I_{520+540}/I_{655}$ ratio also showed no apparent changes for Er@2.6/AgNW hybrids with varied UCNP coverages (Fig. S31†). That is, the surface coverage of the UCNPs on AgNWs (<1 ML) showed almost negligible influence on the coupling of LSPR and UCPL, since the LSPR–UCPL distances were determined by the shell thickness of UCNPs when the surface coverage was below 1 ML.

3.5 Optical measurements from randomly aggregated samples

The single-nanowire method allows us to precisely study the influence of spectrum match, distance, and surface coverage on the coupling between the LSPR effect of the single AgNW and the UCPL process of the attached UCNPs. In sharp contrast, collecting the total signals from a large number of randomly aggregated samples will not provide such high-fidelity signals and suffer from large distributions of critical properties for different samples, even those prepared in one batch (*e.g.*, the diameters of different AgNWs prepared in the same batch). In addition, the interferences of the absorption and scattering of mixed AgNWs (or other NPs) are also inevitable in the collective spectra of mixed samples. For example, we can reveal the influence of the spectrum match on the LSPR enhancement of UCPL on a single-nanowire scale with the assistance of the quasi *in situ* selective etching method (Fig. 3

and 4). However, the collective signals from mixed samples (even prepared in one batch) cannot provide such credible results. As shown in Fig. S32,† two typical samples consisting of several Tm@2.1/AgNWs exhibited similar collective scattering spectra for AgNWs, which may suggest a similar enhancement on UCPL and thus a similar blue-to-red ratio of the UCPL emission. However, the acquired blue-to-red ratios for these samples were significantly different from each other. A similar phenomenon could also be observed in the study of mixed Er@2.6/AgNW samples (Fig. S33†). These results clearly suggest the imprecision for quantifying the LSPR–UCPL coupling from a large number of mixed samples with intrinsic and inevitable drawbacks. Therefore, the single nanowire optical measurement protocol, as well as the quasi *in situ* selective etching method, showed much higher reliability and accuracy for the study of the LSPR-enhancement of UCPL, and provided a powerful method for quantifying the LSPR–UCPL coupling.

4. Conclusions

In summary, we developed a surface modification and chemical assembly protocol for the preparation of UCNPs/AgNW hybrids with precisely tunable parameters, including LSPR–UCPL spectrum match, distances, and surface UCNP coverages. We also developed a single-nanowire scale optical acquisition setup assisted by the quasi *in situ* selective etching method to precisely explore the influences of these critical parameters on the coupling of LSPR and UCPL. Our results proved that AgNWs could significantly enhance the UCPL intensity of Tm-/Er-doped UCNPs, showing a strong dependence on the spectrum match and the distances between the LSPR and UCPL components. Especially, compared with acquiring the collective signals from a large number of mixed samples with inevitable challenges in broad sample distributions and mutual interferences, our single-nanowire characterization and the quasi *in situ* selective methods provide a superior approach to quantifying LSPR–UCPL coupling and evaluating the key parameters with high accuracy and fidelity. With these advantages, our developed chemical synthesis and optical measurement methods may find more applications in studying LSPR and/or UCPL materials, leading to a deeper understanding of the coupling mechanism of surface plasmon and photoluminescence processes.

Author contributions

A.X.Y. designed the research. X.S. synthesized the hybrids and conducted the structure analysis. X.S. conducted the luminescence studies. L.W.C., Z.J.J.Z., J.N.L., N.Z., T.A.B., Y.C.H., W.Y. G., D.L., S.Q.W., Z.L.Y., and H.Z.H assisted with the material synthesis, characterization, and optical measurements. X.S and A.X.Y. co-wrote the paper. A.X.Y. supervised the research. All authors discussed the results and assisted during manuscript preparation.

Conflicts of interest

There are no conflicts to declare.

Acknowledgements

The authors acknowledge the Analytical and Testing Center of BIT for technical support. This work was supported by the National Natural Science Foundation of China (No. 21971012), the Beijing Municipal Natural Science Foundation (JQ20007), and the Beijing Institute of Technology Research Fund Program for Young Scholars.

References

1 C. C. Mi, J. P. Zhang, H. Y. Gao, X. L. Wu, M. Wang, Y. F. Wu, Y. Q. Di, Z. R. Xu, C. B. Mao and S. K. Xu, Multifunctional Nanocomposites of Superparamagnetic (Fe_3O_4) and NIR-Responsive Rare Earth-Doped Up-Conversion Fluorescent ($NaYF_4$:Yb,Er) Nanoparticles and Their Applications in Biolabeling and Fluorescent, *Nanoscale*, 2010, **2**, 1057.

2 H. Dong, L.-D. Sun and C.-H. Yan, Energy Transfer in Lanthanide Upconversion Studies for Extended Optical Applications, *Chem. Soc. Rev.*, 2015, **44**, 1608–1634.

3 J. F. Suyver, A. Aebischer, D. Biner, P. Gerner, J. Grimm, S. Heer, K. W. Krämer, C. Reinhard and H. U. Güdel, Novel Materials Doped with Trivalent Lanthanides and Transition Metal Ions Showing Near-Infrared to Visible Photon Upconversion, *Opt. Mater.*, 2005, **27**, 1111–1130.

4 Y. Song, G. X. Liu, X. T. Dong, J. X. Wang, W. S. Yu and J. M. Li, Au Nanorods@$NaGdF_4$/Yb^{3+},Er^{3+} Multifunctional Hybrid Nanocomposites with Upconversion Luminescence, Magnetism, and Photothermal Property, *J. Phys. Chem. C*, 2015, **119**, 18527–18536.

5 T. Liang, Z. Li, P. P. Wang, F. Z. Zhao, J. Z. Liu and Z. H. Liu, Breaking Through the Signal-to-Background Limit of Upconversion Nanoprobes Using a Target-Modulated Sensitizing Switch, *J. Am. Chem. Soc.*, 2018, **140**, 14696–14703.

6 C. Würth, S. Fischer, B. Grauel, A. P. Alivisatos and U. Resch-Genger, Quantum Yields, Surface Quenching, and Passivation Efficiency for Ultrasmall Core/Shell Upconverting Nanoparticles, *J. Am. Chem. Soc.*, 2018, **140**, 4922–4928.

7 Z. L. Qiu, J. Shu and D. P. Tang, Near-Infrared-to-Ultraviolet Light-Mediated Photoelectrochemical Aptasensing Platform for Cancer Biomarker Based on Core-Shell $NaYF_4$:Yb,Tm@TiO_2 Upconversion Microrods, *Anal. Chem.*, 2018, **90**, 1021–1028.

8 W. Zheng, P. Huang, D. T. Tu, E. Ma, H. M. Zhu and X. Y. Chen, Lanthanide-Doped Upconversion Nano-Bioprobes: Electronic Structures, Optical Properties, and Biodetection, *Chem. Soc. Rev.*, 2015, **44**, 1379–1415.

9 J. Zhao, J. H. Gao, W. T. Xue, Z. H. Di, H. Xing, Y. Lu and L. L. Li, Upconversion Luminescence-Activated DNA Nanodevice for ATP Sensing in Living Cells, *J. Am. Chem. Soc.*, 2018, **140**, 578–581.

10 Y. X. Ao, K. H. Zeng, B. Yu, Y. Miao, W. Hung, Z. Z. Yu, Y. H. Xue, T. T. Y. Tan, T. Xu, M. Zhen, X. L. Yang, Y. Zheng and S. B. Gao, An Upconversion Nanoparticle Enables Near Infrared-Optogenetic Manipulation of the Caenorhabditis Elegans Motor Circuit, *ACS Nano*, 2019, **13**, 3373–3386.

11 D. G. Yin, C. C. Wang, J. Ouyang, X. Y. Zhang, Z. Jiao, Y. Feng, K. L. Song, B. Liu, X. Z. Cao, L. Zhang, Y. L. Han and M. H. Wu, Synthesis of a Novel Core-Shell Nanocomposite Ag@SiO_2@Lu_2O_3:Gd/Yb/Er for Large Enhancing Upconversion Luminescence and Bioimaging, *ACS Appl. Mater. Interfaces*, 2014, **6**, 18480–18488.

12 Y. Li, J. L. Tang, D.-X. Pan, L.-D. Sun, C. Y. Chen, Y. Liu, Y.-F. Wang, S. Shi and C.-H. Yan, A Versatile Imaging and Therapeutic Platform Based on Dual-Band Luminescent Lanthanide Nanoparticles toward Tumor Metastasis Inhibition, *ACS Nano*, 2016, **10**, 2766–2773.

13 B. Dong, S. Xu, J. Sun, S. Bi, D. Li, X. Bai, Y. Wang, L. P. Wang and H. W. Song, Multifunctional $NaYF_4$:Yb^{3+}, Er^{3+}@Ag Core/Shell Nanocomposites: Integration of Upconversion Imaging and Photothermal Therapy, *J. Mater. Chem.*, 2011, **21**, 6193.

14 Q. F. Xiao, X. P. Zheng, W. B. Bu, W. Q. Ge, S. J. Zhang, F. Chen, H. Y. Xing, Q. G. Ren, W. P. Fan, K. L. Zhao, Y. Q. Hua and J. L. Shi, A Core/Satellite Multifunctional Nanotheranostic for in Vivo Imaging and Tumor Eradication by Radiation/Photothermal Synergistic Therapy, *J. Am. Chem. Soc.*, 2013, **135**, 13041–13048.

15 B. Shen, S. M. Cheng, Y. Y. Gu, D. R. Ni, Y. L. Gao, Q. Q. Su, W. Feng and F. Y. Li, Revisiting the Optimized Doping Ratio in Core/Shell Nanostructured Upconversion Particles, *Nanoscale*, 2017, **9**, 1964–1971.

16 J. H. Nie, H. Gao, X. Li and S. M. Liu, Upconversion Luminescence Properties of Different Fluoride Matrix Materials $NaREF_4$ (RE: Gd, Lu, Y) Doped with Er^{3+}/Yb^{3+}, *J. Lumin.*, 2018, **204**, 333–340.

17 G. S. Yi and G. M. Chow, Synthesis of Hexagonal-Phase $NaYF_4$:Yb,Er and $NaYF_4$:Yb,Tm Nanocrystals with Efficient Up-Conversion Fluorescence, *Adv. Funct. Mater.*, 2006, **16**, 2324–2329.

18 F. Wang, Y. Han, C. S. Lim, Y. H. Lu, J. Wang, J. Xu, H. Y. Chen, C. Zhang, M. H. Hong and X. G. Liu, Simultaneous Phase and Size Control of Upconversion Nanocrystals through Lanthanide Doping, *Nature*, 2010, **463**, 1061–1065.

19 Y.-F. Wang, L.-D. Sun, J.-W. Xiao, W. Feng, J.-C. Zhou, J. Shen and C.-H. Yan, Rare-Earth Nanoparticles with Enhanced Upconversion Emission and Suppressed Rare-Earth-Ion Leakage, *Chem. – Eur. J.*, 2012, **18**, 5558–5564.

20 F. Zhang, R. C. Che, X. M. Li, C. Yao, J. P. Yang, D. K. Shen, P. Hu, W. Li and D. Y. Zhao, Direct Imaging the Upconversion Nanocrystal Core/Shell Structure at the Subnanometer Level: Shell Thickness Dependence in Upconverting Optical Properties, *Nano Lett.*, 2012, **12**, 2852–2858.

21 H.-X. Mai, Y.-W. Zhang, L.-D. Sun and C.-H. Yan, Highly Efficient Multicolor Up-Conversion Emissions and Their Mechanisms of Monodisperse $NaYF_4$:Yb,Er Core and Core/Shell-Structured Nanocrystals, *J. Phys. Chem. C*, 2007, **111**, 13721–13729.

22 W. Q. Zou, C. Visser, J. A. Maduro, M. S. Pshenichnikov and J. C. Hummelen, Broadband Dye-Sensitized Upconversion of Near-Infrared Light, *Nat. Photonics*, 2012, **6**, 560–564.

23 X. D. Wang, R. R. Valiev, T. Y. Ohulchanskyy, H. Agren, C. H. Yang and G. Y. Chen, Dye-Sensitized Lanthanide-Doped Upconversion Nanoparticles, *Chem. Soc. Rev.*, 2017, **46**, 4150–4167.

24 M. A. Khan and H. Idriss, Advances in Plasmon-Enhanced Upconversion Luminescence Phenomena and Their Possible Effect on Light Harvesting for Energy Applications, *WIREs Energy Environ.*, 2017, **6**, e254.

25 W. H. Park, D. W. Lu and S. Ahn, Plasmon Enhancement of Luminescence Upconversion, *Chem. Soc. Rev.*, 2015, **44**, 2940–2962.

26 M. D. Wu, A. García-Etxarri, A. Salleo and J. A. Dionne, A. Plasmon-Enhanced Upconversion, *J. Phys. Chem. Lett.*, 2014, **5**, 4020–4031.

27 K. W. Krämer, D. Biner, G. Frei, H. U. Güdel, M. P. Hehlen and S. R. Lüthi, Hexagonal Sodium Yttrium Fluoride Based Green and Blue Emitting Upconversion Phosphors, *Chem. Mater.*, 2004, **16**, 1244–1251.

28 Y. S. Liu, D. T. Tu, H. M. Zhu, R. F. Li, W. Q. Luo and X. Y. Chen, A Strategy to Achieve Efficient Dual-Mode Luminescence of Eu^{3+} in Lanthanides Doped Multifunctional $NaGdF_4$ Nanocrystals, *Adv. Mater.*, 2010, **22**, 3266–3271.

29 F. Wang, J. Wang and X. G. Liu, Direct Evidence of a Surface Quenching Effect on Size-Dependent Luminescence of Upconversion Nanoparticles, *Angew. Chem., Int. Ed.*, 2010, **49**, 7456–7460.

30 H. J. Chen, L. Shao, Q. Li and J. F. Wang, Gold Nanorods and Their Plasmonic Properties, *Chem. Soc. Rev.*, 2013, **42**, 2679–2724.

31 H. Q. Li, Q. Q. Deng, B. Liu, J. H. Yang and B. Wu, Fabrication of Core@Spacer@Shell Au Nanorod@mSiO_2@Y_2O_3:Er Nanocomposites with Enhanced Upconversion Fluorescence, *RSC Adv.*, 2016, **6**, 13343–13348.

32 H. Wang, M. C. Li, Z. Yin, T. X. Zhang, X. Chen, D. L. Zhou, J. Y. Zhu, W. Xu, H. N. Cui and H. W. Song, Remarkable Enhancement of Upconversion Luminescence on Cap-Ag/PMMA Ordered Platform and Trademark Anticounterfeiting, *ACS Appl. Mater. Interfaces*, 2017, **9**, 37128–37135.

33 Z. J. Wang, C. Wang, Q. Y. Han, G. Wang, M. D. Zhang, J. Zhang, W. Gao and H. R. Zheng, Metal-Enhanced Upconversion Luminescence of $NaYF_4$:Yb/Er with Ag Nanoparticles, *Mater. Res. Bull.*, 2017, **88**, 182–187.

34 X. D. Zhang, B. Li, M. M. Jiang, L. M. Zhang and H. P. Ma, Core-Spacer-Shell Structured $NaGdF_4$:Yb^{3+}/Er^{3+}@$NaGdF_4$ @Ag Nanoparticles for Plasmon-Enhanced Upconversion Luminescence, *RSC Adv.*, 2016, **6**, 36528–36533.

35 Z. Yin, D. L. Zhou, W. Xu, S. B. Cui, X. Chen, H. Wang, S. H. Xu and H. W. Song, Plasmon-Enhanced Upconversion Luminescence on Vertically Aligned Gold Nanorod Monolayer Supercrystals, *ACS Appl. Mater. Interfaces*, 2016, **8**, 11667–11674.

36 C. Zhang and J. Y. Lee, Synthesis of Au Nanorod@Amine-Modified Silica@Rare-Earth Fluoride Nanodisk Core-Shell-Shell Heteronanostructures, *J. Phys. Chem. C*, 2013, **117**, 15253–15259.

37 A. L. Feng, M. L. You, L. M. Tian, S. Singamaneni, M. Liu, Z. F. Duan, T. J. Lu, F. Xu and M. Lin, Distance-Dependent Plasmon-Enhanced Fluorescence of Upconversion Nanoparticles using Polyelectrolyte Multilayers as Tunable Spacers, *Sci. Rep.*, 2015, **5**, 7779.

38 Z. J. Wang, W. Gao, R. B. Wang, J. Shao, Q. Y. Han, C. Wang, J. Zhang, T. T. Zhang, J. Dong and H. R. Zheng, Influence of SiO_2 Layer on the Plasmon Quenched Upconversion Luminescence Emission of Core-Shell $NaYF_4$:Yb,Er@SiO_2@Ag Nanocomposites, *Mater. Res. Bull.*, 2016, **83**, 515–521.

39 B. Zhao, N. Qi, K.-Q. Zhang and X. Gong, Fabrication of Freestanding Silk Fibroin Films Containing Ag Nanowires/$NaYF_4$:Yb,·Er Nanocomposites with Metal-Enhanced Fluorescence Behavior, *Phys. Chem. Chem. Phys.*, 2016, **18**, 15289–15294.

40 D. Piatkowski, N. Hartmann, T. Macabelli, M. Nyk, S. Mackowski and A. Hartschuh, A. Silver Nanowires as Receiving-Radiating Nanoantennas in Plasmon-Enhanced Up-Conversion Processes, *Nanoscale*, 2015, **7**, 1479–1484.

41 W. Feng, L.-D. Sun and C.-H. Yan, Ag Nanowires Enhanced Upconversion Emission of $NaYF_4$:Yb,Er Nanocrystals via a Direct Assembly Method, *Chem. Commun.*, 2009, 4393–4395.

42 K. Park, K. Jung, S. J. Kwon, H. S. Jang, D. J. Byun, I. K. Han and H. Ko, Plasmonic Nanowire-Enhanced Upconversion Luminescence for Anticounterfeit Devices, *Adv. Funct. Mater.*, 2016, **26**, 7836–7846.

43 H. Dong, L.-D. Sun, Y.-F. Wang, J.-W. Xiao, D. T. Tu, X. Y. Chen and C.-H. Yan, Photon Upconversion in Yb^{3+}-Tb^{3+} and Yb^{3+}-Eu^{3+} Activated Core/Shell Nanoparticles with Dual-Band Excitation, *J. Mater. Chem. C*, 2016, **4**, 4186–4192.

44 A. G. Dong, X. C. Ye, J. Chen, Y. J. Kang, T. Gordon, J. M. Kikkawa and C. B. Murray, A Generalized Ligand-Exchange Strategy Enabling Sequential Surface Functionalization of Colloidal Nanocrystals, *J. Am. Chem. Soc.*, 2011, **133**, 998–1006.

45 J. Jung, H. Lee, I. Ha, H. Cho, K. K. Kim, J. Kwon, P. Won, S. Hong and S. H. Ko, Highly Stretchable and Transparent Electromagnetic Interference Shielding Film Based on Silver Nanowire Percolation Network for Wearable Electronics Applications, *ACS Appl. Mater. Interfaces*, 2017, **9**, 44609–44616.

46 D. R. Cai, J. Zhou, P. P. Duan, G. Y. Luo, Y. Y. Zhang, F. Y. Fu and X. D. Liu, A Hierarchical Structure of L-Cysteine/Ag NPs/Hydrogel for Conductive Cotton Fabrics with High Stability against Mechanical Deformation, *Cellulose*, 2018, **25**, 7355–7367.

47 M. Luo, H. W. Huang, S.-I. Choi, C. Zhang, R. R. D. Silva, H.-C. Peng, Z.-Y. Li, J. Y. Liu, Z. K. He and Y. N. Xia, Facile Synthesis of Ag Nanorods with No Plasmon Resonance Peak in the Visible Region by Using Pd Decahedra of 16 nm in Size as Seeds, *ACS Nano*, 2015, **9**, 10523–10532.

48 K. Zhan, R. Su, S. H. Bai, Z. H. Yu, N. Cheng, C. L. Wang, S. Xu, W. Liu, S. S. Guo and X.-Z. Zhao, One-Pot Stirring-Free Synthesis of Silver Nanowires with Tunable Lengths and Diameters via a Fe^{3+} & Cl^- Co-Mediated Polyol Method and Their Application as Transparent Conductive Films, *Nanoscale*, 2016, **8**, 18121–18133.

49 D. Xing, C.-C. Lin, P. Won, R. Xiang, T.-P. Chen, A. S. A. Kamal, Y.-C. Lee, Y.-L. Ho, S. Maruyama, S. H. Ko, C.-W. Chen and J.-J. Delaunay, Metallic Nanowire Coupled $CsPbBr_3$ Quantum Dots Plasmonic Nanolaser, *Adv. Funct. Mater.*, 2021, 2102375.

50 S. J. Kasani, K. Curtin and N. Q. Wu, A Review of 2D and 3D Plasmonic Nanostructure Array Patterns: Fabrication, Light Management and Sensing Applications, *Nanophotonics*, 2019, **8**, 2065–2089.

